

Exploring the Relative Contribution of the MJO and ENSO to Midlatitude Subseasonal Predictability

Kirsten J. Mayer^{1*}, William E. Chapman^{1*}, William A. Manriquez²

¹U.S. National Science Foundation National Center for Atmospheric Research

²Metropolitan State University of Denver

*These authors contributed equally

Key Points:

- An interpretable neural network is used to decompose contributions of MJO and ENSO to North Pacific subseasonal circulation predictability.
- ENSO alone is overall more useful than the MJO for subseasonal predictions across various lead times and predictand averaging windows.
- Unique MJO events, that provide enhanced subseasonal predictability during ENSO neutral conditions, are identified.

Corresponding authors: Kirsten J. Mayer; William E. Chapman, kjmayer@ucar.edu; wchapman@ucar.edu

14 Abstract

15 Here we explore the relative contribution of the Madden-Julian Oscillation (MJO)
16 and El Niño Southern Oscillation (ENSO) to midlatitude subseasonal predictive skill of
17 upper atmospheric circulation over the North Pacific, using an inherently interpretable
18 neural network applied to pre-industrial control runs of the Community Earth System
19 Model version 2. We find that this interpretable network generally favors the state of
20 ENSO, rather than the MJO, to make correct predictions on a range of subseasonal lead
21 times and predictand averaging windows. Moreover, the predictability of positive cir-
22 culation anomalies over the North Pacific is comparatively lower than that of their neg-
23 ative counterparts, especially evident when the ENSO state is important. However, when
24 ENSO is in a neutral state, our findings indicate that the MJO provides some predic-
25 tive information, particularly for positive anomalies. We identify three distinct evolu-
26 tions of these MJO states, offering fresh insights into opportune forecasting windows for
27 MJO teleconnections.

28 Plain Language Summary

29 Weather is hard to predict with longer forecast leads. Here, we use a data-driven
30 statistical model to dissect tropical sources of predictability on 2 week to 2 month mid-
31 latitude upper-level variability. This model was constructed so that we can identify the
32 relative contributions of two tropical phenomena important for predictability on these
33 timescales. Namely, we use the Madden-Julian Oscillation (MJO) and the El Niño South-
34 ern Oscillation (ENSO) as predictor variables, two phenomena that provide a telecon-
35 necting signal from the tropics to midlatitude variability. We find that the ENSO sig-
36 nal alone consistently provides more forecast predictability than the MJO. However, when
37 ENSO is not active, the MJO provides distinct windows of forecast opportunity, partic-
38 ularly for anomalously anticyclonic events. We identify three evolutions of the MJO which
39 offer new insights into forecasting weather at long forecast leads.

40 1 Introduction

41 Forecasting for the subseasonal timescale (often defined as 2 weeks through 2 months)
42 has received considerable attention over the last decade (White et al., 2017; Mariotti et
43 al., 2020; Merryfield et al., 2020; White et al., 2021). These timescales are particularly
44 difficult to predict as generally neither atmospheric initial conditions nor slower vary-
45 ing boundary conditions provide sufficient information to make useful predictions (Vi-
46 tart et al., 2012, 2017; Mariotti et al., 2020). Unfortunately, this is also a timescale in
47 which many public and private sectors seek information to make informed, actionable
48 decisions in order to save lives and property (White et al., 2017, 2021). One way to gar-
49 ner skill on these timescales is to harness predictive skill from specific modes of variabil-
50 ity known to provide enhanced subseasonal predictability when the mode is active – termed
51 forecasts of opportunity (Mariotti et al., 2020). One such mode of variability that has
52 gathered considerable attention in the subseasonal community is the Madden-Julian Os-
53 cillation (MJO; Madden & Julian, 1971, 1972, 1994).

54 The MJO consists of two oppositely signed zonally oriented convective anomalies
55 that propagate from the Indian Ocean to the central Pacific, completing a cycle every
56 20 to 90 days. The associated upper-level circulation anomalies can interact with the sub-
57 tropical jet, exciting quasi-stationary Rossby waves (Hoskins & Ambrizzi, 1993), which
58 influence midlatitude circulation anomalies on subseasonal timescales. Following specific
59 phases (i.e. locations) of the MJO, this teleconnection can lead to improved prediction
60 skill on subseasonal timescales (Tseng et al., 2018). The MJO teleconnection has been
61 shown to manifest as a Pacific North American (PNA) - like system. In its positive phase,
62 the PNA is characterized by a deepened Aleutian Low, and increased Canadian High,

63 and a deepened Florida low pattern which extends into the Atlantic (Wallace & Gut-
64 zler, 1981). The Aleutian Low limb of the PNA, in particular, is responsible for greater
65 downstream effects of precipitation and temperature anomalies across the whole of North
66 America. In observations, the growth of the PNA anomaly is dominated by barotropic
67 energy conversion from the zonally asymmetric climatological flow in the North Pacific
68 storm track (e.g., Feldstein, 2002; Frederiksen, 1983; Simmons et al., 1983). However,
69 a primary mode of Aleutian Low growth is also from excitation by tropical heating, such
70 as from the MJO or El Niño Southern Oscillation (ENSO) Hoskins & Ambrizzi (1993);
71 Sardeshmukh & Hoskins (1988).

72 ENSO is an interannual coupled ocean-atmosphere mode in the tropical Pacific (Tren-
73 berth, 1997), and the primary mode of tropical variability. However, it can also influ-
74 ence the subseasonal timescale through its impact on the MJO (Hendon et al., 1999; Kessler,
75 2001; Pohl & Matthews, 2007) and the basic state in which MJO teleconnections prop-
76 agate (Namias, 1986; Moon et al., 2011; Takahashi & Shirooka, 2014), ultimately impact-
77 ing the MJO’s influence in the midlatitudes (Stan et al., 2017; Henderson & Maloney,
78 2018; Tseng et al., 2020; Arcodia et al., 2020) and subsequent subseasonal prediction skill
79 (Johnson, Collins, Feldstein, L’Heureux, & Riddle, 2014; L. Wang & Robertson, 2019).
80 Further, recent work suggests ENSO may play a main role in changes to midlatitude sub-
81 seasonal predictability in a future, warmer climate (Mayer & Barnes, 2022). While ENSO
82 is often used for seasonal prediction (e.g., Gibson et al., 2021; Winkler et al., 2001), there
83 is also considerable literature that highlights ENSO teleconnections as a driver of mid-
84 latitude subseasonal variability, particularly in boreal winter by also modulating the Aleu-
85 tian Low (e.g., Kumar & Hoerling, 1998; Chapman et al., 2021). Notably, the ENSO tele-
86 connection exhibits significant evolution throughout a season. This dynamic evolution
87 contributes to heightened predictability and diverse surface responses, contingent on the
88 time of year and the strength of the background flow (the mid-latitude jet). Consequently,
89 this lends support to the suggestion that ENSO could rival the MJO as a dominant driver
90 of subseasonal forecast skill (Chapman et al., 2021).

91 These results raise the question as to the relative role of the MJO and ENSO in
92 midlatitude subseasonal predictability. Johnson, Collins, Feldstein, L’Heureux, & Rid-
93 dle (2014) showed that skillful subseasonal forecasts can be derived solely using the state
94 of the MJO and ENSO. However, given the time-scale of these two modes of variabil-
95 ity, the utility of the MJO for midlatitude predictability dwindles as a function of lead-
96 time while the ENSO utility remains a reliable source of longer range predictability. This
97 study seeks to further elucidate the relative roles of both ENSO and MJO for midlat-
98 itude subseasonal forecasting using a more complex and interpretable statistical tech-
99 nique. We explore a range of forecast lead times and predictand averaging window lengths
100 to investigate the relative role of these tropical drivers of subseasonal predictability for
101 a variety of forecast criteria.

102 In recent years, neural networks have been shown to be a powerful statistical tool
103 for the atmospheric sciences due to their ability to identify non-linear, physical relation-
104 ships within large amounts of data (Toms et al., 2020, 2021; Labe & Barnes, 2022; Mar-
105 tin et al., 2022; Davenport & Duffenbaugh, 2021; Gordon et al., 2021). For example, on
106 subseasonal timescales, explainable neural networks were demonstrated to identify sub-
107 seasonal forecasts of opportunity using the network’s “confidence” in a given prediction
108 as well as the associated tropical sources of predictability through explainability tech-
109 niques (Mayer & Barnes, 2021). Here we utilize network confidence and an interpretable
110 neural network architecture known as a Neural Additive Model (Agarwal et al., 2020;
111 Gordon et al., 2023), to disentangle the relative contributions of the MJO and ENSO
112 to subseasonal predictability over the North Pacific in the pre-industrial control simu-
113 lations from the Community Earth System Model. Specifically, we create two artificial
114 neural networks, one of which receives an MJO index while the other receives an ENSO
115 index. The predictions from these two networks are linearly combined to generate the

116 final prediction for the sign of Z500 anomaly over the North Pacific on subseasonal timescales.
 117 This allows for the decomposition of a network’s prediction into the respective contri-
 118 butions from ENSO and MJO. We find that information about the state of ENSO alone
 119 is overall more important than that of the MJO for subseasonal predictability of North
 120 Pacific circulation in the pre-industrial simulations. However, the state of the MJO still
 121 provides important information particularly for shorter lead time predictions of positive
 122 Z500 anomalies during network-identified forecasts of opportunity.

123 2 Data & Methods

124 2.1 Data

125 We leverage the Community Earth System Model version 2 (CESM2) pre-industrial
 126 control run (CESM2-PI) from model years 100-400 from the CMIP6 experiment suite
 127 (Danabasoglu et al., 2020). CESM2-PI has interactive land, coupled ocean with biogeo-
 128 chemistry, interacting sea-ice and non-evolving land ice, and constant 1850’s CO₂ forc-
 129 ing. The model’s resolution is nominally 1 degree, with 32 vertical levels. A full descrip-
 130 tion of the CESM2-PI runs can be found in Danabasoglu et al. (2020). From those years
 131 we select the daily geopotential height at 500 hPa (Z500), sea surface temperature (SST),
 132 and zonal wind at 200 hPa and 850 hPa (U200 and U850, respectively). We then sep-
 133 arate the data into three independent data sets: training [model years 100-200], valida-
 134 tion [model years 201-300], and testing [model years 301-400]. 100 years of training data
 135 was found sufficient to have the machine learning models fully converge on optimal so-
 136 lutions, meaning, adding more data did not significantly change resultant learned net-
 137 work weights. There is consensus that the eastern Pacific teleconnections associated with
 138 MJO and ENSO peak during the boreal winter (e.g., Philander, 1985; Henderson et al.,
 139 2016; Chapman et al., 2021). Therefore, we focus our investigation exclusively on this
 140 seasonal period, restricting our model training and analysis to input dates ranging from
 141 November 1st to February 28th. Consequently, the forecasts extend until March 30th,
 142 with a lead time of 30 days.

143 The practical relevance of this study relies on an accurate representation of the an-
 144 alyzed modes of variability in CESM2-PI. The primary rationale for scrutinizing predictabil-
 145 ity within CESM2-PI, rather than relying on observations, is to augment the size of the
 146 datasets used for training, testing, and validating the neural networks. CESM2-PI is rec-
 147 ognized as a cutting-edge model, particularly in its representation of the MJO and ENSO,
 148 along with their associated North Pacific teleconnections. Numerous studies have eval-
 149 uated the accuracy of this representation (Danabasoglu et al., 2020; J. Wang et al., 2022;
 150 Capotondi et al., 2020). To further corroborate the fidelity of these teleconnections, with
 151 particular attention to the task presented to the neural network, we present the frequency
 152 of anomalous Z500 signs 5-9 days after an active MJO in phases 3/4 and 6/7 in the sup-
 153plementary material (Fig. S1), and compare that representation to that in ECMWF’s
 154 version 5 reanalysis product (ERA5, Hersbach et al., 2020). It is clear that the model
 155 represents the MJO teleconnection well, capturing the dominate location and sign of the
 156 Z500 anomalous for the two active teleconnection phases of the MJO.

157 Additionally, the same suite of forecast variables was downloaded from ERA5 (1979-
 158 2020), to verify that the ML models results are valid on a global reanalysis product. The
 159 ERA5 product is regridded to the common CESM2 grid prior to any reanalysis using
 160 a bilinear interpolation scheme (Zhuang et al., 2018).

161 **2.2 Methods**

162 **2.2.1 MJO, ENSO, & Aleutian Low Indices**

163 We follow the methods of Lin et al. (2008) for calculation of the real-time multi-
 164 variate MJO indices (RMM1 and RMM2) in the CESM2-PI runs. Starting from the un-
 165 filtered observed daily averaged data of the OLR and zonal wind at 850-hPa and 200-
 166 hPa from model years 100-400, the time-mean, and the first three harmonics of the daily
 167 climatology are removed at every grid-point. Next, the time-series is filtered, by remov-
 168 ing the grid-point time-mean of the previous 120 days. Removing the previous 120-day
 169 average eliminates most of the interannual variability, including the effects of ENSO. A
 170 meridional band average is then taken from 15°S to 15°N for the three fields. Each vari-
 171 able is then normalized by its own zonal average of temporal standard deviation, the fields
 172 are combined and decomposed and the two leading EOFs are retained. The resulting struc-
 173 tures of the EOF modes are very similar to Wheeler & Hendon (2004, not shown).

174 The ENSO index is computed by employing a rolling 90-day window and a cosine
 175 latitude weighted average of the Sea Surface Temperature (SST) anomaly within the con-
 176 ventional Nino3.4 region [5°N-5°S and 170°W-120°W]. The SST anomaly is determined
 177 by subtracting a 60-day rolling average centered on each day of the year.

178 The target of the neural network is the sign of the Aleutian Low index. The Aleu-
 179 tian Low index is a representation the anomalous geopotential height at 500 hPa in the
 180 eastern North Pacific and is determined via the following process: Initially, a 60-day rolling
 181 average centered climatology is subtracted from the raw geopotential height data, with
 182 each center point corresponding the model day of year. Then the anomalous index within
 183 the target region [30°N to 60°N and 190°W to 250°W], is computed via a cosine latitude
 184 weighted average. Finally, the target averaging window is established by applying a for-
 185 ward rolling mean to the daily index data, using the desired target window length (2-
 186 28 days).

187 Finally, previous studies have indicated that the wintertime evolution of the ba-
 188 sic state is non-trivial (Newman & Sardeshmukh, 1998) and thus tropically derived, east-
 189 ern Pacific, teleconnections [which feed off the barotropic energy conversion provided by
 190 the divergence of the background jet] vary greatly (Chapman et al., 2021; Sardeshmukh
 191 & Hoskins, 1988). Thus, we also input the day of the year (DOY), which is represented
 192 as a linearly increasing value spanning from the first of November to the final day of Febru-
 193 ary, encompassing all input days. The DOY index is subsequently normalized, ensuring
 194 it maintains a zero mean and a standard deviation of unity, prior to its incorporation
 195 into the neural network.

196 **2.2.2 Interpretable Neural Network**

197 Figure 1 shows a schematic of the interpretable neural network specifically constructed
 198 to dissect the relative contributions of the MJO and ENSO to subseasonal predictabil-
 199 ity over the North Pacific. Following the general architecture laid out in Gordon et al.
 200 (2023), two artificial neural networks are combined at the output layer through a linear
 201 combination to create the final output prediction. In our applications, both networks are
 202 tasked to predict the sign of the 500 hPa geopotential height anomaly averaged over the
 203 North Pacific at the target lead. However, the top network (Figure 1a) only receives in-
 204 formation about the state of ENSO and its evolution throughout 15 days prior (here-
 205 after referred to as the ENSO-network) while the bottom network only receives the RMM1
 206 and RMM2 index values and their evolution throughout the 15 days prior (Figure 1b;
 207 hereafter referred to as the MJO-network). Additionally, each network receives the DOY
 208 associated with t_0 as input so that it may also learn variability in sources of predictabil-
 209 ity within the boreal winter season. The final predictions are taken as the linear com-
 210 bination of the outputs of the individual networks, meaning that the network must learn

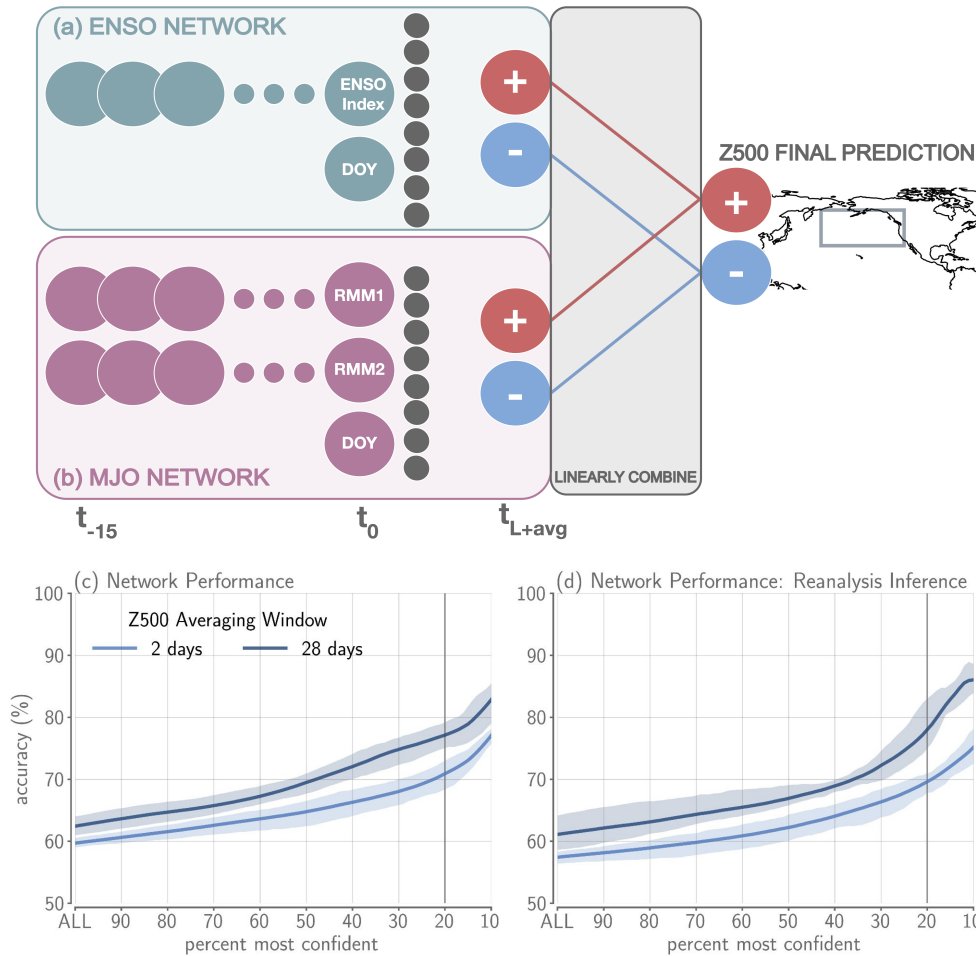


Figure 1. Schematic of the interpretable neural network architecture. Input into the (a) ENSO-network includes the ENSO index at t_0 plus the 15 days prior (t_{-15}) and associated normalized day of year (DOY) at t_0 to predict the sign of the Z500 anomaly averaged over North Pacific (grey rectangle) at a specified lead (t_{L+avg} , where “L” indicates the lead time and “avg” indicates the Z500 temporal averaging window length). The (b) MJO-network is constructed similarly but instead inputs RMM1 and RMM2 rather than the ENSO index. The predictions from each network are linearly combined (grey shaded box) to make the final network prediction. The bottom two panels include network performance [accuracy] across confidence thresholds for the (c) testing dataset and (d) ERA5 reanalysis. The light/dark blue lines represent the mean accuracy at each confidence level across all lead times (shading) for a Z500 averaging window of 2 days/28 days

211 to strategically weight its contribution to the final prediction. Therefore, the individual
 212 output of each neural network can be considered its contribution to a prediction, allow-
 213 ing interpretation of the specific role of each predictor (i.e., ENSO or MJO) in the net-
 214 work’s skill.

215 To explore the impact of lead and predictand temporal averaging on the source of
 216 predictabilty, we train separate neural networks for leads ranging from 5 to 30 days and
 217 predictand temporal averaging windows of 2 to 28 days. Furthermore, we train five net-
 218 works, each with a different random seed per lead and averaging window combination,
 219 to assess the network’s sensitivity to random initialization weights. Minimal differences
 220 between random initializations are observed, leading us to present the results as aver-
 221 ages across the five networks.

222 Both the ENSO- and MJO- networks have one hidden layer with eight nodes and
 223 use the rectified linear unit (ReLU) activation function. We note that increasing the com-
 224 plexity of either network does not impact the results [not shown]. To train the model,
 225 we use a batch size of 32, categorical crossentropy as the loss function and the Adam Op-
 226 timizer (Kingma & Ba, 2014) for gradient descent with a learning rate of 0.001. The learn-
 227 ing rate is initially held constant for the first 19 epochs and then reduced by 90% after
 228 each epoch to help minimize the loss. To reduce overfitting to the training data, train-
 229 ing is completed after the validation loss does not improve for 20 epochs, at which time
 230 the network weights are reverted to 20 epochs prior. The softmax activation function
 231 is applied to the final layer of the total-network (Figure 1) so that the output values sum
 232 to one and represent a network estimation of likelihood, or “confidence”. Previous re-
 233 search has shown that network confidence can be used to identify forecasts of opportu-
 234 nity when accuracy increases with confidence (Mayer & Barnes, 2021), allowing us to
 235 explore the contributions of the MJO and ENSO for all predictions and during network-
 236 identified forecasts of opportunity. Here, we define confident predictions as the 20% most
 237 confident following (Mayer & Barnes, 2022).

238 ***2.2.3 Quantifying Relative Contribution***

239 We employ two methods to quantify the relative contribution of the ENSO- and
 240 MJO- networks to the total-network predictions. The first explores the frequency that
 241 the final, total prediction is correctly predicted by a specific network while incorrectly
 242 predicted by the other. This illuminates how often either the ENSO- *or* MJO- network
 243 solely contributes to the correct total-network prediction while the other network acts
 244 incorrectly.

245 The second metric quantifies the percentage of the total-network accuracy provided
 246 by either the ENSO- or MJO- network through permutation importance McGovern et
 247 al. (2019). Permutation importance is a technique used to remove relationships between
 248 the input and output through randomly shuffling the input data. The subsequent de-
 249 crease in network performance can then be attributed to the importance of that input
 250 data to the prediction. To calculate the importance (percentage of accuracy) contributed
 251 by the ENSO-network, we randomly shuffle the ENSO index testing samples (retaining
 252 the 15 day memory), calculate the accuracy of the total-network with the randomly shuf-
 253 fled data, and compare it to the accuracy of the total-network without shuffled data. To
 254 calculate the percentage of accuracy contributed by the MJO-network, we apply the same
 255 technique, but shuffle the RMM indices. We note that the random shuffling does not ac-
 256 count for memory between samples, and therefore, the network contribution to the to-
 257 tal accuracy could be larger.

258 3 Results

259 3.1 Network Performance

260 To evaluate network performance, we calculate the accuracy of the network on the
 261 testing data across confidence levels (Figure 1c). The testing data is randomly subset
 262 to an equal number of positive and negative anomalies so that random chance is 50%
 263 for all predictions ($N \approx 11,500$; 100% most confident). Across the range of Z500 averag-
 264 ing windows (lines) and lead times (shading), the network performs better than random
 265 change at $\geq 60\%$ accuracy. We include the two extreme averaging windows (2 and 28
 266 days) for ease of visualization, however, the other averaging windows fall within these
 267 two curves. As network confidence increases, the accuracy of the network increases as
 268 well, indicating the network is able to identify periods of enhanced predictability (Fig-
 269 ure 1c). Further, we find similar performance when the network is evaluated on reanal-
 270 ysis data (Figure 1d), suggesting the network is identifying physically relevant forecasts
 271 of opportunity for subseasonal predictability of Z500 anomalies over the North Pacific
 272 (Mayer & Barnes, 2021).

273 Previous work has also detailed the importance of the basic state evolution through-
 274 out boreal winter on tropically forced teleconnection propagation and its potential for
 275 improved subseasonal predictability (Newman & Sardeshmukh, 1998; Chapman et al.,
 276 2021, e.g.). Therefore, to account for any within season evolution of ENSO or MJO tele-
 277 connections to North Pacific predictability, DOY is included as an input into the net-
 278 work. We find that when the network is correct (grey histograms in Figure 2), the fre-
 279 quency of predictions are generally consistent across DOY with a slight increase towards
 280 the latter end of the season across leads 7 through 28 days. However, when the network
 281 is also confident (purple histograms in Figure 2), the frequency of predictions increases
 282 at the latter end of boreal winter. We note that the purple histograms become flatter
 283 with lead time (i.e. more early winter predictions) since longer lead time predictions made
 284 near the beginning of boreal winter are forecasting for the latter part of the season. These
 285 results indicate that the network has identified the latter half of boreal winter as a prefer-
 286 able period for enhanced subseasonal predictability, consistent with previous research
 287 (Newman & Sardeshmukh, 1998; Chapman et al., 2021). In other words, the network
 288 is able to identify a "sub-seasonal" evolution of subseasonal predictability sourced from
 289 the MJO and ENSO.

290 To ensure the network does not solely rely on DOY to classify confident predictions,
 291 we also train neural networks without DOY information, and find similar MJO and ENSO
 292 contribution results (not shown). To maximize samples, the following analysis examines
 293 predictions throughout the season, rather than only during the latter half of boreal win-
 294 ter.

295 3.2 MJO- & ENSO-Network Contributions

296 Due to the construction of the neural network, the relative contributions from each
 297 network to the final predictions can be quantified. Specifically, we calculate the frequency
 298 that either the ENSO- (teal) or MJO- (purple) network solely contributes to a correct,
 299 final prediction (Figure 3a). The frequency that both networks contribute to a correct
 300 prediction is also included in grey, so that the sum of the teal, purple and grey lines at
 301 a specific lead and Z500 averaging window is 100%. Lighter (darker) colors denote shorter
 302 (longer) temporal Z500 averaging windows.

303 Overall, we find that the ENSO-network alone (teal) contributes more frequently
 304 to correct predictions than the MJO-network alone (purple) for almost all leads and Z500
 305 averaging windows. At shorter Z500 averaging windows (2 and 7 days), the MJO-network
 306 contributes more frequently until about a lead of 14-18 days, after which the ENSO-network
 307 becomes more frequently correct regardless of Z500 averaging windows. The most fre-

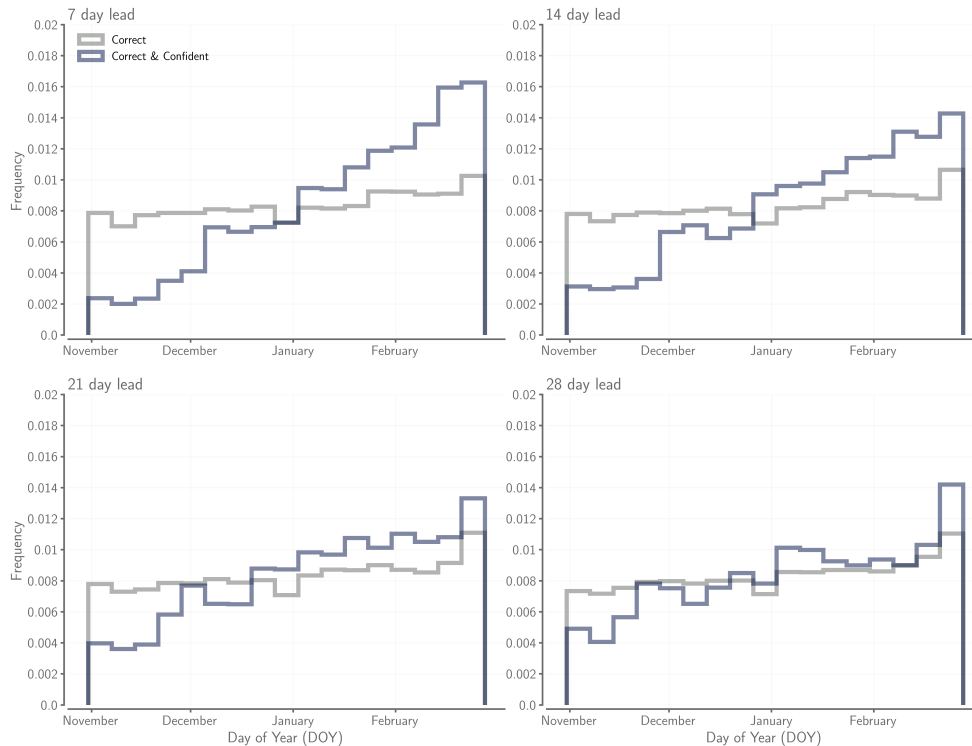


Figure 2. Frequency of a correct (grey) and confident (purple) network predictions by day of year (DOY) for a lead of 7, 14, 21, and 28 days across all Z500 averaging windows.

308 frequently correct network combination is when *both* networks agree on the correct predic-
 309 tion (grey lines). However, the information provided by the ENSO state begins to con-
 310 tribute as frequently at leads greater than 21 days and longer averaging windows (darker
 311 teal lines). In general, as either the Z500 averaging window or lead time increases, the
 312 ENSO-network alone contributes more frequently to a correct prediction than the MJO-
 313 network. These results show that while the MJO-state is important for making predic-
 314 tions, ENSO plays a greater role in making correct subseasonal predictions for the ma-
 315 jority of lead times and Z500 averaging windows.

316 If we further subset the predictions into correct and confident predictions (i.e. network-
 317 identified forecasts of opportunity), a similar though more exaggerated, story emerges.
 318 After a lead of 7 days, the ENSO-network contributes more frequently to correct and con-
 319 fident predictions than the MJO-network, regardless of Z500 averaging window (Figure
 320 3b). At shorter leads the most frequent correct, confident predictions still occur when
 321 *both* the ENSO- and MJO-network correctly contribute to the predictions. However, the
 322 ENSO-network alone rivals these frequencies after a lead of 21 days. These results again
 323 demonstrate that the ENSO-network alone is generally more useful for correct (and con-
 324 fident) subseasonal predictions than the MJO-network.

325 When confident and correct predictions are further separated into positive and nega-
 326 tive Z500 anomaly predictions, the contributions become more nuanced (Fig. 3b.1- b.2).
 327 For negative predictions, the ENSO-network more frequently contributes to correct, con-
 328 fident predictions than the MJO-network, regardless of lead time or averaging window.
 329 However, when examining positive predictions [note change to y-axis limits], the MJO-
 330 network alone contributes to correct, confident predictions more frequently than the ENSO-
 331 network at 5-7 day leads and Z500 averaging windows of 2 and 7 days (Fig. 3b.2). This

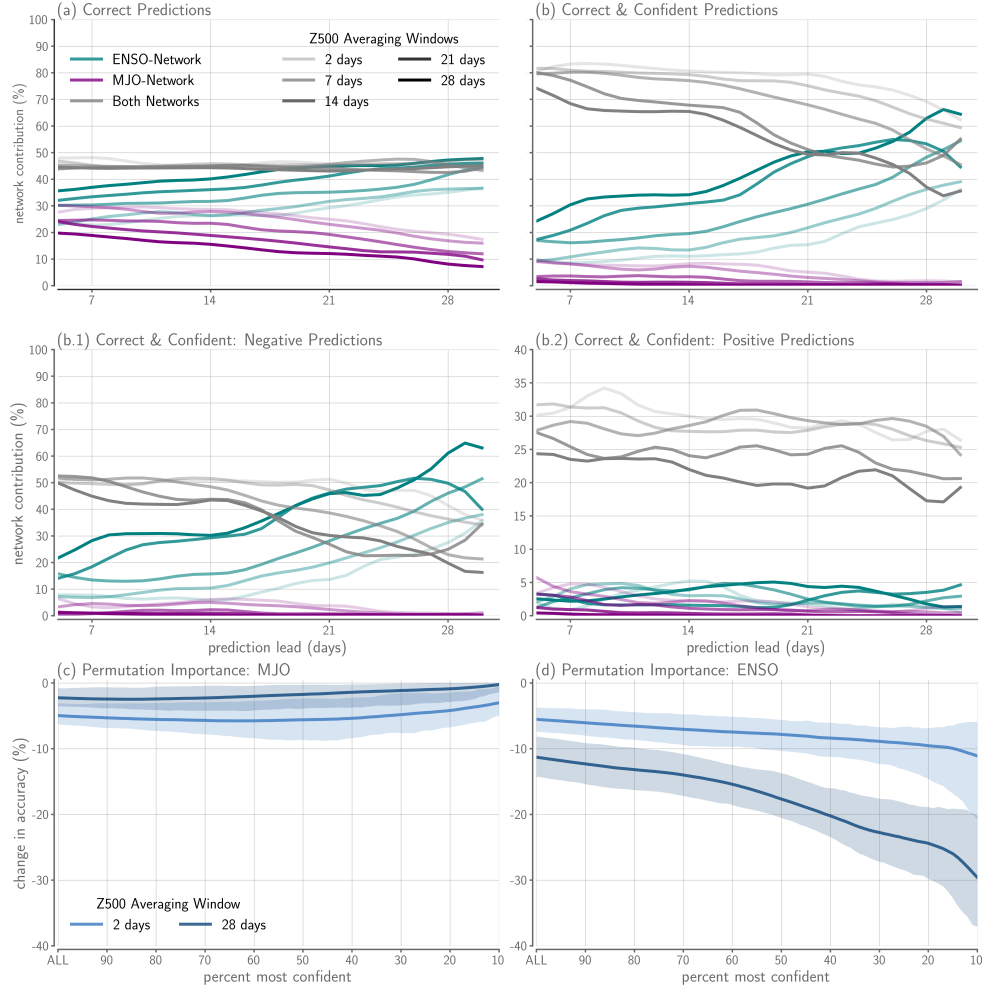


Figure 3. The frequency of a correct prediction provided by *either* the MJO- (purple) or ENSO-network (teal) or by *both* MJO- and ENSO-networks (grey) for each prediction lead. Lighter (darker) lines indicate shorter (longer) Z500 averaging windows. (b) As in (a) but for correct and confident predictions, which is further divided into (b.1) positive and (b.2) negative Z500 predictions [note different y-axis limits]. Lines are smoothed with a 3 day triangle filter for ease of interpretation. (c,d) Change in accuracy across confidence thresholds after permuting (c) RMM and (d) ENSO index input. The light/dark blue lines represent the mean of a 2 day/28 day Z500 averaging window across all lead times and the associated range of change in accuracy is represented by the shading.

332 suggests the MJO state is especially important for subseasonal prediction of anomalously
 333 high Z500 at shorter leads and averaging windows, particularly when the ENSO state
 334 is not useful (e.g. ENSO neutral conditions).

335 The utility of the MJO-network to the total network can be further elucidated when
 336 the prediction problem is, for example, constructed with a lead of 10 days and a Z500
 337 averaging window of 5 days. We find that 42% of correct, confident positive Z500 anomaly
 338 predictions are periods with ENSO neutral conditions, when the tropical ocean should
 339 have the least control on the extratropical eastern Pacific. This is in stark contrast to
 340 confident, correct negative predictions which only occur in ENSO neutral states in 12%
 341 of cases. With that said, we note that negative predictions, of which the ENSO-network
 342 dominates, are overall more frequently confident and correct than positive predictions
 343 (Fig. 3b.1).

344 The results of the relative network contributions generally suggests the ENSO-network
 345 is the main contributor to correct (and confident) predictions. However, the MJO-network
 346 shows its utility for positive predictions when the network is correct and confident. We
 347 can further explore the impact of the MJO-network and ENSO-network on prediction
 348 skill through permutation importance (Figure 3c,d). In particular, we can quantify the
 349 contribution of the ENSO-network to the accuracy of the total network (Figure 3d) by
 350 randomly shuffling the input into the ENSO-network. In doing so, we separate the con-
 351 nection between the predictor and predictand, and thus, the predictors importance for
 352 making correct predictions. We find that across lead (shading) and Z500 averaging win-
 353 dow (lines), the ENSO-network contributes between 5-12% for all predictions and close
 354 to 40% when the network is very confident. When permutation importance is instead
 355 applied to the MJO-network (Figure 3c), this contribution is about 1-5% across confi-
 356 dent thresholds. We again only include the two extreme Z500 averaging windows for vi-
 357 sualization, however, the other averaging window results lie within these curves. This
 358 further demonstrates that information provided by the ENSO-network is more impor-
 359 tant for higher skill, particularly at high confidence values (i.e. during forecasts of op-
 360 portunity), compared to the MJO-network.

361 **3.2.1 MJO-Network Importance**

362 In general, our network indicates that ENSO is a more consistent provider of forecast
 363 skill of Z500 anomalies over the North Pacific. Nevertheless, there are specific time
 364 frames when the MJO-network provides important information for predicting Z500. To
 365 delve deeper into the MJO's optimal state for subseasonal predictability of Z500 in the
 366 North Pacific, K-means clustering is employed on the input features of the MJO network
 367 (RMM1 and RMM2). For brevity, we focus on a single lead time and averaging window
 368 (10 days and 5 days, respectively). This was found as a lead time and averaging window
 369 of relative peak importance for MJO driven predictability (Fig. 3b). This analysis fo-
 370 cuses on instances when the network is confident and accurate, only during neutral ENSO
 371 conditions. We employ elbow and silhouette analysis to ascertain the optimal number
 372 of clusters for both positive and negative confident and correct predictions (Fig. S2, Rousseeuw,
 373 1987). These methods offer a quantitative measure of how well-defined and separated
 374 the clusters are, providing insights into the cohesion within each cluster and the distinc-
 375 tiveness between clusters. This ensures a more nuanced evaluation of the clustering struc-
 376 ture and reinforces our confidence in the appropriateness of the chosen number of clus-
 377 ters (3; Figure S2). The silhouette analysis shows clearly separated clusters which en-
 378 hances the reliability of our clustering results, contributing to the overall robustness of
 379 our analysis. We then take a mean across the temporal dimension of each cluster to form
 380 a cluster composite of the input MJO RMM1/RMM2 predictor variables. Composites
 381 of the three clusters, for positive (top row) and negative (bottom row) Z500 anomaly pre-
 382 dictions, are shown in figure 4.

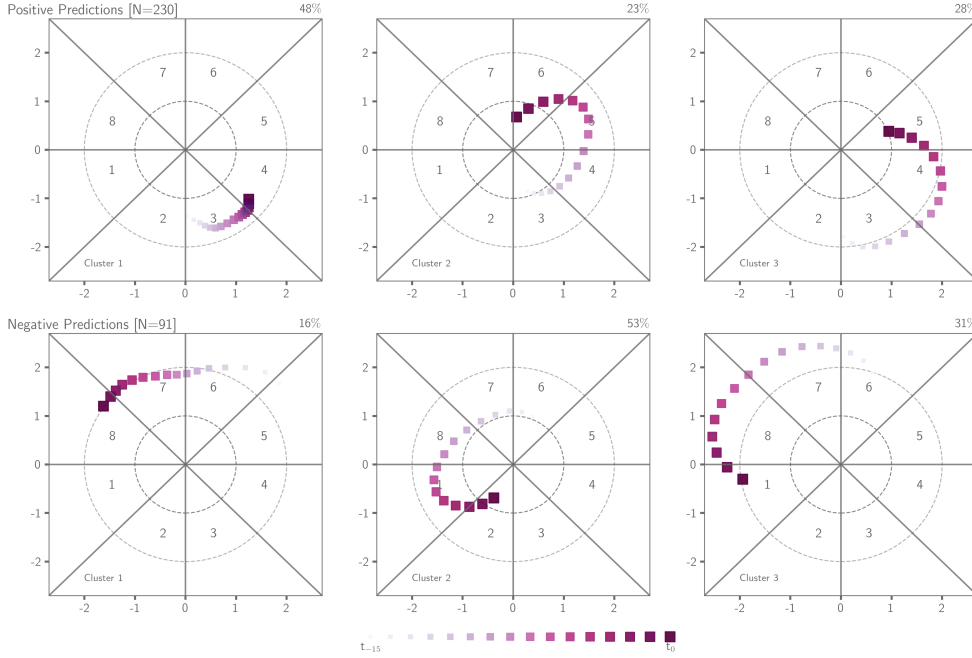


Figure 4. Composite clusters of MJO events when predictions are confident, correct, and ENSO is in a neutral state for anomalously high (top row) and anomalously low (bottom row) Aleutian Low states. Forecast lead is 10 days and a Z500 averaging window of 5 days. The RMM indices progress in time from light- [t_{-15}] to dark- [t_0] colors.

383 Firstly, we observe the frequency of events in which ENSO is neutral and the network
 384 exhibits both confident and correct predictions, represented as an N value in each
 385 row. Positive predictions are approximately 2.5 times more likely than negative events
 386 to exhibit this forecast condition (N=230 vs. N=91). This implies that the network demon-
 387 strates greater confidence and accuracy when forecasting positive Z500 anomalies dur-
 388 ing ENSO neutral states. Consequently, the MJO proves to be a more effective predic-
 389 tor (in CESM2-PI) in phases 3/4, where downstream Rossby wave dispersion leads to
 390 positive Z500 North Pacific anomalies. It is important to note that this does not nec-
 391 essarily imply that positive anomalies are universally more predictable at the subseasonal
 392 range, as the total number of confident, correct negative predictions is higher than those
 393 predicting a positive state (refer to the discussion of Fig. 3 for further details), and this
 394 is largely driven by ENSO positive events.

395 Positive predictions (row 1; high Z500 anomalies) show three distinct developing
 396 MJO states. Each developing MJO state is consistent with the phases that lead to a down-
 397 stream positive Z500 anomaly (peaking in phases 3/4/5), demonstrating that the neu-
 398 ral network has identified a physically justifiable link between the MJO and North Pa-
 399 cific circulation. Every cluster is above the threshold for active MJO events (1 sigma,
 400 inner dashed circle), and cluster 3 has periods which are above the 2 standard deviation
 401 threshold (97.5 percentile; outer dashed circle). Meaning, extremely anomalous events
 402 more consistently produce downstream extra-tropical Z500 anomalies. Cluster 1 shows
 403 a persistent anomaly in which the MJO stalls in between phases 3 and 4. These persis-
 404 tent cases have been previously identified as exciting a greater teleconnection response
 405 than fast moving MJO events (Yadav & Straus, 2017; Yadav et al., 2024). Finally, clus-
 406 ters 2 and 3 show events that are anomalously strong which then decay into MJO neu-
 407 tral states as they move towards initialization time. This is logical as MJO phase 6/7/8

408 is associated with a negative Z500 anomaly and thus would negate the current Z500 pos-
409 sive prediction at subseasonal forecast leads. To the author’s knowledge, this is a unique
410 aspect of this analysis showing that selective extremely anomalous MJO phases which
411 then decay to a neutral MJO state can lead to enhanced subseasonal forecast skill, by
412 *not* sparking MJO induced Rossby wave destructive interference. For the sake of brevity,
413 we will simply note that the negative Z500 predictions (row2; low Z500 anomalies), largely
414 mirror the findings found in the positive Z500 predictions.

415 The authors acknowledge that the MJO and ENSO indices along with the day of
416 year are the sole information available to the network for making predictions. Keeping
417 this limitation in mind, in summary, the subseasonal predictability of the Eastern North
418 Pacific Z500 anomaly is predominantly influenced by highly active or persistent MJO
419 events during neutral ENSO conditions. Larger anomalies result in increased predictabil-
420 ity, and MJO events with substantial anomalies that subsequently transition into neu-
421 tral states significantly contribute to subseasonal forecast skill.

422 4 Conclusion

423 This study aims to use an interpretable neural network to enhance the scientific
424 understanding of the contribution of two tropical modes of variability to subseasonal pre-
425 dictability over the North Pacific: the MJO and ENSO. We find the network performs
426 well on both the CESM2-PI testing data and ERA5 reanalysis across the range of lead
427 time and averaging windows evaluated, suggesting the network is able to identify phys-
428 ically relevant sources of predictability. Further, the network is able to identify a late
429 boreal winter preference for enhanced subseasonal predictability (Fig. 2), consistent with
430 previous research which explores the importance of the subseasonal evolution of the back-
431 ground state for teleconnection propagation (e.g., Kumar & Hoerling, 1998; Chapman
432 et al., 2021). This area of predictability research remains relatively unexplored, calling
433 for more focused investigation.

434 Through an analysis of the relative roles of the MJO- and ENSO-networks, we find
435 that forecast lead time and predictand averaging windows have a limited effect on the
436 relative importance of MJO-driven North Pacific variability. ENSO dominates as the pri-
437 mary driver of subseasonal predictability for the majority of lead times and averaging
438 windows, particularly at forecast ranges exceeding 7 days and averaging windows greater
439 than 2 days (Fig. 3b,d). However, the MJO does provide some utility for prediction of
440 positive Z500 anomalies during ENSO neutral states. In particular, persistent and par-
441 ticularly anomalous MJO events that decay before creating destructive interference of-
442 fer the greatest utility for subseasonal predictability from the MJO in this region (Fig.
443 4).

444 The authors acknowledge that we predict the *sign* of the Aleutian Low anomaly
445 and the relative importance of each predictor variable could change if the predictive tar-
446 get is changed to forecasting the magnitude or other, downstream affects of the MJO or
447 ENSO (i.e., two-meter temperature or precipitation). Further, these results are for the
448 CESM2-PI simulation, and therefore, does not account for possible affects from anthro-
449 pogenic climate change. Recent research has shown that the MJO has become and will
450 likely continue to become more predictable in a future climate (Du et al., 2023), which
451 could subsequently improve midlatitude subseasonal skill provided by the MJO. On the
452 other hand, previous research suggests ENSO may be the main tropical driver of future
453 midlatitude subseasonal predictability changes (Mayer & Barnes, 2022). Therefore, fu-
454 ture research should explore how our results may change in a future, warmer climate.

455 Given the chaotic nature of the weather system, a priori identification of particu-
456 larly predictive windows offers a useful way forward for long range forecast skill (Al-
457 bers & Newman, 2019; Mariotti et al., 2020). Ultimately, this paper demonstrates that

458 interpretable neural networks can be used to gain physical insight into predictability, par-
 459 ticularly through dissecting the relative importance of modes of variability thought im-
 460 portant for subseasonal predictability.

461 5 Open Research

462 To promote transparency and reproducibility, all model training scripts and fig-
 463 ures are readily accessible and can be downloaded using the provided code available on
 464 GitHub (<https://github.com/kjmayer/ENSOvsMJO> ; Mayer & Chapman, 2024). Com-
 465 prehensive instructions for each step of this study are documented in the repository’s README
 466 file. The authors leveraged the TensorFlow Python toolbox for machine learning and model
 467 training, a python machine learning environment can be found in this projects’ repos-
 468 itory. All data was produced as a part of the Community Earth System Model’s con-
 469 tribution to the CMIP6 suite and is archived at the U.S. National Science Foundation’s
 470 National Center for Atmospheric Research (NSF NCAR) computational and informa-
 471 tion systems lab (<https://www2.cisl.ucar.edu/computing-data/data/cmip6-data-sets-glade>).
 472 Raw ERA5 Reanalysis data can be obtained on the NSF NCAR Research Data Archive
 473 at: <https://rda.ucar.edu/datasets/ds633.0/>. Intermediate data files that can be lever-
 474 aged to run every neural network and produce every plot specified in the github repo are
 475 stored at NCAR’s Geoscience Data Exchange (Chapman & Mayer, 2024).

476 Acknowledgments

477 The work conducted by KJM is supported by the U.S. Department of Energy, Office of
 478 Science, Office of Biological & Environmental Research (BER), Regional and Global Model
 479 Analysis (RGMA) component of the Earth and Environmental System Modeling Pro-
 480 gram under Award Number DE-SC0022070 and National Science Foundation (NSF) IA
 481 1947282. WEC received M²LInES research funding by the generosity of Eric and Wendy
 482 Schmidt by recommendation of the Schmidt Futures program. Further, this material is
 483 based upon work supported by the U.S. National Science Foundation under Grant No.
 484 AGS - 2230301 (NSF SOARS). Additionally, this work was supported by the U.S. Na-
 485 tional Science Foundation National Center for Atmospheric Research (NSF NCAR), which
 486 is a major facility sponsored by the NSF under Cooperative Agreement No. 1852977.
 487 Any opinions, findings, and conclusions or recommendations expressed in this material
 488 are those of the author(s) and do not necessarily reflect the views of the U.S. National
 489 Science Foundation.

490 We thank Dr. Emily Gordon for her insight and advice on using this interpretable
 491 neural networks.

492 References

- 493 Agarwal, R., Melnick, L., Frosst, N., Zhang, X., Lengerich, B., Caruana, R., & Hin-
 494 ton, G. (2020, April). Neural additive models: Interpretable machine learning
 495 with neural nets.
- 496 Albers, J. R., & Newman, M. (2019). A priori identification of skillful extratropical
 497 subseasonal forecasts. *Geophysical Research Letters*, *46*(21), 12527–12536.
- 498 Arcodia, M. C., Kirtman, B. P., & Siqueira, L. S. P. (2020). How MJO teleconnec-
 499 tions and ENSO interference impacts US precipitation. *J. Clim.*.
- 500 Capotondi, A., Deser, C., Phillips, A., Okumura, Y., & Larson, S. (2020). Enso and
 501 pacific decadal variability in the community earth system model version 2. *Journal*
 502 *of Advances in Modeling Earth Systems*, *12*(12), e2019MS002022.
- 503 Chapman, W. E., & Mayer, K. J. (2024). *Data for Exploring the Relative Contri-*
 504 *bution of the MJO and ENSO to Midlatitude Subseasonal Predictability [Dataset]*.
 505 doi: <https://doi.org/10.5065/f21v-ya03>

- 506 Chapman, W. E., Subramanian, A. C., Xie, S.-P., Sierks, M. D., Ralph, F. M., &
507 Kamae, Y. (2021). Monthly modulations of enso teleconnections: Implications for
508 potential predictability in north america. *Journal of Climate*, *34*(14), 5899–5921.
- 509 Danabasoglu, G., Lamarque, J.-F., Bacmeister, J., Bailey, D., DuVivier, A., Ed-
510 wards, J., ... others (2020). The community earth system model version 2
511 (cesm2). *Journal of Advances in Modeling Earth Systems*, *12*(2), e2019MS001916.
- 512 Davenport, F. V., & Diffenbaugh, N. S. (2021, July). Using machine learning to
513 analyze physical causes of climate change: A case study of U.S. midwest extreme
514 precipitation. *Geophys. Res. Lett.*
- 515 Du, D., Subramanian, A. C., Han, W., Chapman, W. E., Weiss, J. B., & Bradley,
516 E. (2023). Increase in mjo predictability under global warming. *Nature Climate
517 Change*, 1–7.
- 518 Feldstein, S. B. (2002). Fundamental mechanisms of the growth and decay of the
519 pna teleconnection pattern. *Quarterly Journal of the Royal Meteorological So-
520 ciety: A journal of the atmospheric sciences, applied meteorology and physical
521 oceanography*, *128*(581), 775–796.
- 522 Frederiksen, J. (1983). A unified three-dimensional instability theory of the onset of
523 blocking and cyclogenesis. ii. teleconnection patterns. *Journal of Atmospheric Sci-
524 ences*, *40*(11), 2593–2609.
- 525 Gibson, P. B., Chapman, W. E., Altinok, A., Delle Monache, L., DeFlorio, M. J., &
526 Waliser, D. E. (2021). Training machine learning models on climate model output
527 yields skillful interpretable seasonal precipitation forecasts. *Communications Earth
528 & Environment*, *2*(1), 159.
- 529 Gordon, E. M., Barnes, E. A., & Davenport, F. V. (2023). Separating internal and
530 forced contributions to near term sst predictability in the cesm2-le. *Environmental
531 Research Letters*.
- 532 Gordon, E. M., Barnes, E. A., & Hurrell, J. W. (2021, November). Oceanic
533 harbingers of pacific decadal oscillation predictability in CESM2 detected by
534 neural networks. *Geophys. Res. Lett.*, *48*(21).
- 535 Henderson, S. A., & Maloney, E. D. (2018, July). The impact of the Madden–Julian
536 oscillation on High-Latitude winter blocking during el niño–southern oscillation
537 events. *J. Clim.*, *31*(13), 5293–5318.
- 538 Henderson, S. A., Maloney, E. D., & Barnes, E. A. (2016). The influence of the
539 madden–julian oscillation on northern hemisphere winter blocking. *Journal of Cli-
540 mate*, *29*(12), 4597–4616.
- 541 Hendon, H. H., Zhang, C., & Glick, J. D. (1999, August). Interannual variation
542 of the Madden–Julian oscillation during austral summer. *J. Clim.*, *12*(8), 2538–
543 2550.
- 544 Hersbach, H., Bell, B., Berrisford, P., Hirahara, S., Horányi, A., Muñoz-Sabater, J.,
545 ... others (2020). The era5 global reanalysis. *Quarterly Journal of the Royal
546 Meteorological Society*, *146*(730), 1999–2049.
- 547 Hoskins, B. J., & Ambrizzi, T. (1993, June). Rossby wave propagation on a realistic
548 longitudinally varying flow. *J. Atmos. Sci.*, *50*(12), 1661–1671.
- 549 Johnson, N. C., Collins, D. C., Feldstein, S. B., L’Heureux, M. L., & Riddle, E. E.
550 (2014, February). Skillful wintertime north american temperature forecasts out
551 to 4 weeks based on the state of ENSO and the MJO. *Weather Forecast.*, *29*(1),
552 23–38.
- 553 Johnson, N. C., Collins, D. C., Feldstein, S. B., L’Heureux, M. L., & Riddle, E. E.
554 (2014). Skillful wintertime north american temperature forecasts out to 4 weeks
555 based on the state of enso and the mjo. *Weather and Forecasting*, *29*(1), 23–38.
- 556 Kessler, W. S. (2001, July). EOF representations of the Madden–Julian oscillation
557 and its connection with ENSO. *J. Clim.*, *14*(13), 3055–3061.
- 558 Kingma, D. P., & Ba, J. (2014). Adam: A method for stochastic optimization. *arXiv
559 preprint arXiv:1412.6980*.

- 560 Kumar, A., & Hoerling, M. P. (1998). Annual cycle of pacific–north american sea-
561 sonal predictability associated with different phases of enso. *Journal of Climate*,
562 *11*(12), 3295–3308.
- 563 Labe, Z. M., & Barnes, E. A. (2022, May). Predicting slowdowns in decadal climate
564 warming trends with explainable neural networks. *Geophys. Res. Lett.*
- 565 Lin, H., Brunet, G., & Derome, J. (2008). Forecast skill of the madden–julian os-
566 cillation in two canadian atmospheric models. *Monthly Weather Review*, *136*(11),
567 4130–4149.
- 568 Madden, R. A., & Julian, P. R. (1971, July). Detection of a 40–50 day oscillation in
569 the zonal wind in the tropical pacific. *J. Atmos. Sci.*, *28*(5), 702–708.
- 570 Madden, R. A., & Julian, P. R. (1972, September). Description of Global-Scale cir-
571 culation cells in the tropics with a 40–50 day period. *J. Atmos. Sci.*, *29*(6), 1109–
572 1123.
- 573 Madden, R. A., & Julian, P. R. (1994, May). Observations of the 40–50-day tropical
574 Oscillation—A review. *Mon. Weather Rev.*, *122*(5), 814–837.
- 575 Mariotti, A., Baggett, C., Barnes, E. A., Becker, E., Butler, A., Collins, D. C., ...
576 Albers, J. (2020, January). Windows of opportunity for skillful forecasts subsea-
577 sonal to seasonal and beyond. *Bull. Am. Meteorol. Soc.*
- 578 Martin, Z. K., Barnes, E. A., & Maloney, E. (2022, May). Using simple, explainable
579 neural networks to predict the Madden-Julian oscillation. *J. Adv. Model. Earth*
580 *Syst.*
- 581 Mayer, K. J., & Barnes, E. A. (2021, May). Subseasonal forecasts of opportunity
582 identified by an explainable neural network. *Geophys. Res. Lett.*
- 583 Mayer, K. J., & Barnes, E. A. (2022, July). Quantifying the effect of climate change
584 on midlatitude subseasonal prediction skill provided by the tropics. *Geophys. Res.*
585 *Lett.*, *49*(14).
- 586 Mayer, K. J., & Chapman, W. E. (2024). *Code (Version 1.0.0) for Exploring the*
587 *Relative Contribution of the MJO and ENSO to Midlatitude Subseasonal Pre-*
588 *dictability [Software]. Zenodo.* Retrieved from [https://github.com/kjmayer/](https://github.com/kjmayer/ENSOvsMJO)
589 [ENSOvsMJO](https://doi.org/10.5281/zenodo.10607685) doi: <https://doi.org/10.5281/zenodo.10607685>
- 590 McGovern, A., Lagerquist, R., Gagne, D. J., Jergensen, G. E., Elmore, K. L., Home-
591 yer, C. R., & Smith, T. (2019). Making the black box more transparent: Under-
592 standing the physical implications of machine learning. *Bulletin of the American*
593 *Meteorological Society*, *100*(11), 2175–2199.
- 594 Merryfield, W. J., Baehr, J., Batté, L., & others. (2020). Current and emerging de-
595 velopments in subseasonal to decadal prediction. *Bulletin of the*
- 596 Moon, J.-Y., Wang, B., & Ha, K.-J. (2011, September). ENSO regulation of MJO
597 teleconnection. *Clim. Dyn.*, *37*(5), 1133–1149.
- 598 Namias, J. (1986, July). Persistence of flow patterns over north america and adja-
599 cent ocean sectors. *Mon. Weather Rev.*, *114*(7), 1368–1383.
- 600 Newman, M., & Sardeshmukh, P. D. (1998). The impact of the annual cycle on the
601 north pacific/north american response to remote low-frequency forcing. *Journal of*
602 *the Atmospheric Sciences*, *55*(8), 1336–1353.
- 603 Philander, S. (1985). El niño and la niña. *Journal of Atmospheric Sciences*, *42*(23),
604 2652–2662.
- 605 Pohl, B., & Matthews, A. J. (2007, June). Observed changes in the lifetime and
606 amplitude of the Madden–Julian oscillation associated with interannual ENSO sea
607 surface temperature anomalies. *J. Clim.*, *20*(11), 2659–2674.
- 608 Rousseeuw, P. J. (1987). Silhouettes: a graphical aid to the interpretation and val-
609 idation of cluster analysis. *Journal of computational and applied mathematics*, *20*,
610 53–65.
- 611 Sardeshmukh, P. D., & Hoskins, B. J. (1988). The generation of global rotational
612 flow by steady idealized tropical divergence. *Journal of the Atmospheric Sciences*,
613 *45*(7), 1228–1251.

- 614 Simmons, A., Wallace, J., & Branstator, G. (1983). Barotropic wave propagation
615 and instability, and atmospheric teleconnection patterns. *Journal of the Atmo-*
616 *spheric Sciences*, *40*(6), 1363–1392.
- 617 Stan, C., Straus, D. M., Frederiksen, J. S., Lin, H., Maloney, E. D., & Schumacher,
618 C. (2017, December). Review of Tropical-Extratropical teleconnections on in-
619 traseasonal time scales: The subseasonal to seasonal (S2S) teleconnection Sub-
620 Project. *Rev. Geophys.*, *55*(4), 902–937.
- 621 Takahashi, C., & Shirooka, R. (2014, September). Storm track activity over the
622 north pacific associated with the Madden-Julian oscillation under ENSO condi-
623 tions during boreal winter. *J. Geophys. Res.*, *119*(18), 10,663–10,683.
- 624 Toms, B. A., Barnes, E. A., & Ebert-Uphoff, I. (2020, September). Physically
625 interpretable neural networks for the geosciences: Applications to earth system
626 variability. *J. Adv. Model. Earth Syst.*, *12*(9).
- 627 Toms, B. A., Kashinath, K., Yang, D., & Prabhat. (2021, July). Testing the re-
628 liability of interpretable neural networks in geoscience using the Madden–Julian
629 oscillation. *Geosci. Model Dev.*, *14*(7), 4495–4508.
- 630 Trenberth, K. E. (1997). The definition of el nino. *Bull. Am. Meteorol. Soc.*, *78*(12),
631 2771–2778.
- 632 Tseng, K.-C., Barnes, E. A., & Maloney, E. D. (2018, January). Prediction of
633 the midlatitude response to strong Madden-Julian oscillation events on S2S time
634 scales: PREDICTION OF Z500 AT S2S TIME SCALES. *Geophys. Res. Lett.*,
635 *45*(1), 463–470.
- 636 Tseng, K.-C., Maloney, E., & Barnes, E. A. (2020, May). The consistency of MJO
637 teleconnection patterns on interannual time scales. *J. Clim.*, *33*(9), 3471–3486.
- 638 Vitart, F., Ardilouze, C., Bonet, A., Brookshaw, A., Chen, M., Codorean, C., ...
639 Zhang, L. (2017, January). The subseasonal to seasonal (S2S) prediction project
640 database. *Bull. Am. Meteorol. Soc.*, *98*(1), 163–173.
- 641 Vitart, F., Robertson, A. W., & Anderson, D. L. T. (2012, January). Subseasonal to
642 seasonal prediction project: Bridging the gap between weather and climate. *WMO*
643 *Bull.*, *61*(61).
- 644 Wallace, J. M., & Gutzler, D. S. (1981). Teleconnections in the geopotential height
645 field during the northern hemisphere winter. *Monthly weather review*, *109*(4),
646 784–812.
- 647 Wang, J., Kim, H., & DeFlorio, M. J. (2022). Future changes of pna-like mjo tele-
648 connections in cmip6 models: Underlying mechanisms and uncertainty. *Journal of*
649 *Climate*, *35*(11), 3459–3478.
- 650 Wang, L., & Robertson, A. W. (2019, May). Week 3–4 predictability over the united
651 states assessed from two operational ensemble prediction systems. *Clim. Dyn.*,
652 *52*(9), 5861–5875.
- 653 Wheeler, M. C., & Hendon, H. H. (2004). An all-season real-time multivariate mjo
654 index: Development of an index for monitoring and prediction. *Monthly weather*
655 *review*, *132*(8), 1917–1932.
- 656 White, C. J., Carlsen, H., Robertson, A. W., Klein, R. J. T., Lazo, J. K., Kumar,
657 A., ... Zebiak, S. E. (2017, July). Potential applications of subseasonal-to-
658 seasonal (S2S) predictions. *Met. Apps*, *24*(3), 315–325.
- 659 White, C. J., Domeisen, D. I. V., Acharya, N., Adefisan, E. A., Anderson, M. L.,
660 Aura, S., ... Wilson, R. G. (2021, November). Advances in the application and
661 utility of subseasonal-to-seasonal predictions. *Bull. Am. Meteorol. Soc.*, *-1*(aop),
662 1–57.
- 663 Winkler, C. R., Newman, M., & Sardeshmukh, P. D. (2001). A linear model of win-
664 tertime low-frequency variability. part i: Formulation and forecast skill. *Journal of*
665 *climate*, *14*(24), 4474–4494.
- 666 Yadav, P., Garfinkel, C. I., & Domeisen, D. I. (2024). The role of the stratosphere in
667 teleconnections arising from fast and slow mjo episodes. *Geophysical Research Let-*

668 *ters*, 51(1), e2023GL104826.

669 Yadav, P., & Straus, D. M. (2017). Circulation response to fast and slow mjo
670 episodes. *Monthly Weather Review*, 145(5), 1577–1596.

671 Zhuang, J., Dussin, R., Jüling, A., & Rasp, S. (2018). xesmf: Universal regridder for
672 geospatial data. *Zenodo [code]*, 10.